SINERGI Vol. 28, No. 2, June 2024: 251-258
http://publikasi.mercubuana.ac.id/index.php/sinergi
http://doi.org/10.22441/sinergi.2024.2.005

A simplified dental caries segmentation using Half U-Net for a teledentistry system

Trie Maya Kadarina[1], Zendi Iklima[1*], Rinto Priambodo[1], Riandini[2], Rika Novita Wardhani[2], Sulis Setiowati[2], Mohd Taufik Jusoh[3]
[1]Department of Electrical Engineering, Faculty of Engineering, Universitas Mercu Buana, Indonesia
[2]Department of Mechanical Engineering, Politeknik Negeri Jakarta, Indonesia
[3]Department of Electrical and Electronic Engineering, Faculty of Engineering, National Defence University of Malysia, Malaysia

Abstract
High-reliability diagnostic equipment efficiently supported by a computer-based diagnostics system. For instance, a computational approach establishes a model that can diagnose diseases. Artificial intelligence has been applied to aid in the field of medical imaging. Classification, prediction, and localisation of lesions or dental caries greatly minimise the load and difficulties for clinical practitioners. In this study, U-Net architectures are simplified to propose the feature reduction of the decoder layers. This simplification of U-Net architectures is utilised for segmented dental caries images. This paper simplified the U-Net decoder layers into the level of blocks Half-UNet (X_{De}^{4}) and Half-UNet (X_{De}^{3}). The Half-UNet structural model surpasses the U-shaped structural model in terms of efficiency and segmentation capabilities. The simplification of the UNet architecture outperformed using Half-UNet X_{De}^{4} 0.83% of the dice coefficient. The Half-UNet design is able to preserve model performance in segmenting actual images and ground truth against expected ground truth.

Keywords:
Dental Caries;
Half U-Net;
Image Segmentation;
Teledentistry System;

Article History:
Received: July 27, 2023
Revised: November 26, 2023
Accepted: December 4, 2024
Published: June 2, 2024

Corresponding Author:
Zendi Iklima
Department of Electrical Engineering, Faculty of Engineering, Universitas Mercu Buana, Indonesia
Email:
zendi.iklima@mercubuana.ac.id

INTRODUCTION

Dental caries is a progressive dental condition that, if left untreated, can cause serious damage to other teeth, perhaps leading to tooth loss. Dental caries is a bacterial infection of the teeth [1]. Caries can be caused by improperly consuming foods and drinks containing fructose, sucrose, and glucose, which increase the onset of dental caries. Caries result from a never-ending cycle of demineralization and remineralization [2]. Caries can also be found in black and yellow. Caries symptoms may include dental pain, tooth loss, and tooth inflammation. The standard categorizes dental caries depending on their location as well as the damaged tooth. Caries can be classified depending on the degree of lesions on the tooth and positional categorization. The classification is based on the effect of caries on the amount of dentin and enamel. Incipient caries are situations in which less than half of the enamel depth is damaged. This is considered moderate caries when the enamel is more than halfway impacted but does not come into contact with the dentin. Advanced caries are distinguished by their progression to the dentin region, whereas severe caries expand beyond halfway through the dentin and even enter the pulp [3]. Improved hygiene practices, early identification of caries, and supportive therapy may be able to slow or stop the growth of the problem. Clinically, the major approaches for identifying dental caries are visual-tactile examination and dental radiography.

Increasing the number of dentist clinics is one step toward preventing and treating dental diseases. However, most dental clinics are

dispersed across the city core. This makes dental treatment difficult for people in rural areas. Technological developments in the telemedicine branch can facilitate dental health services such as screening, consultation, diagnosis, and recommendations for healing through information technology. Thus, teledentistry has a major impact on the problem of dental disease in rural communities. This can save costs and patient healing time. Teledentistry has a significant role in improving oral health care in dentistry while enhancing access to telemedicine through digital and communication technologies. In contrast to conventional clinical approaches, teledentistry's progressive information and communication technologies have been proving more cost-effective, precise, and adept at providing remote assistance to clinicians. Teledentistry encompasses communication technology for exchanging diagnostic or treatment information among practitioners seeking guidance, direction, supervision, or mentorship in dealing with dental issues [4].

However, Caries' approximations are difficult to distinguish due to their location, which makes clinical evaluation difficult. Erroneous interpretations might hamper the diagnostic process. Leveraging computational methods and technology can assist dentists in evaluating caries. A computer-based diagnostics system is more efficient for supporting high-reliability diagnostic equipment. A mathematical model of disease diagnosis is established using a computer's analytical and computation abilities.

Furthermore, accurately classifying, predicting, and locating lesions related to this disease can substantially alleviate the workload and challenges clinical doctors face. Over the last few decades, artificial intelligence has been applied to bolster the medical imaging domain. Deep learning is the most common computation method used for automatic learning based on substantial medical imaging datasets as feature extraction vectors, namely Convolutional Neural Networks (CNN) [5]. CNN has been shown to be highly effective in computer vision applications such as object, face, and activity detection, tracking, and three-dimensional mapping and localization. Medical segmentation and diagnosis is one of the most significant applications of image processing and pattern recognition technologies [6].

Early detection of dental caries is usually utilized in dentistry. The collected data set consists of 74 images divided into two labels: cavities and non-cavities. By adjusting the hyperparameter, the Deep CNN (DCNN) model has been trained to obtain a maximum accuracy of 71.43% [7]. Model performance can be optimized, for example, by increasing the number of datasets, tuning the hyperparameters, or using pre-trained model. Several pre-trained models were trained to classify cavities and non-cavities. In 100 iterations, VGG16, VGG19, InceptionV3, and ResNet50 were successfully trained with 99.37%, 98.48%, 99.89%, and 98.01% accuracy, respectively [8]. The technology will provide a novel way for recognizing and categorizing various types of teeth, such as underlying oral anomalies, fixed partial dentures, and impacted teeth. Faster-RCNN was trained using OPG datasets and achieved an accuracy of 91.03% [9]. Another pre-trained model was evaluated for classifying caries and non-caries labels. EfficientNet-B0, DenseNet-121, and ResNet-50 performed over 562 panoramic images. When compared to EfficientNet-B0 and DenseNet-121, the ResNet-50 model performed slightly better. The accuracy of this model was 92.00%, the sensitivity was 87.33%, and the F1-score was 91.61%. This result explains how a deep learning model diagnosed dental caries with high accuracy and reliability [10].

An investigation was conducted to assess the diagnostic performance of deep learning in segmenting occlusal, proximal, and cervical caries lesions on panoramic radiographs. The Dental Caries Detection Network (DCDNet) was designed to successfully segment 504 anonymous panoramic radiographs. DCDNet utilized a multi-predicted output (MPO) structure in the optimized last layer. Extensive experimental analyses resulted in an average F1 score of 62.79%, with the state-of-the-art segmentation models reaching the highest average F1 score of 15.69% [11]. In order to perform panoramic X-ray segmentation, CNN was additionally trained on the annotated data. The 1.000-image collection is organized into 14 classifications, with each class indicating a different dental condition. An efficient residual factorized ConvNet (ERFNet) was performed across 200 epochs, producing 98% accuracy, 98% precision, 91% recall, and 93% F1 score [12].

Computer-aided clinic applications have seen significant technological advancements due to deep learning, enabling lesion detection and classification, automatic image segmentation, radiographic feature extraction, and image reconstruction. These systems deliver reliable diagnostic guidance by

optimizing AI-related technology, aiding radiologists in making clinical decisions and easing their workload. Patients and providers also benefit from time savings. Significantly, artificial intelligence-based systems can effectively lower barriers in medical centers lacking radiologists and address the uneven distribution of medical resources. The segmentation of intraoral radiographs has been studied by dividing 500 intraoral radiograph images into five different diagnoses: tooth decays, crowns, pulp, restoration material, and root-filling material. The U-Net architecture was performed using the F1 score, sensitivity, and precision results of the study, respectively: 0.8818–0.8235–0.9491, crown; 0.9629–0.9285–1, pulp; 0.9631–0.9843–0.9429, with restoration material; and 0.9714–0.9622–0.9807 was obtained as 0.9722–0.9459–1 for the root filling material [13].

Extensive efforts have been invested in exploring deep learning techniques for image segmentation, focusing on dental X-ray images. For instance, Mask RCNN and U-Net were utilized to perform instance segmentation, addressing challenges such as low contrast in dental X-rays. A lightweight deep learning method was proposed for dental X-ray image segmentation to facilitate deployment on edge devices. This lightweight approach and various existing lightweight deep learning methods underwent training using a dataset of panoramic dental X-ray images. By utilizing 1500 panoramic dental X-ray images (256x256), which contain ten categories, the lightweight method achieved the best performance in terms of IoU (0,804) and dice (0,89) [14]. A proposed U-Net convolutional network was employed to perform segmentation on 10 dental X-ray images. The dataset was augmented, generating a total of 5000 images, all 224x224 pixels. The evaluation of the segmentation utilized ground-truth images. The U-Net convolutional network segmentation and the ground truth had only two grayscale intensity values (255 and 0), so the accuracy, sensitivity, and specificity values were all the same. The U-Net convolutional network has proven its proficiency in accurately identifying and outlining dental structures from X-ray images achieving an outstanding average segmentation accuracy of 97.60% [15].

In the realm of medical image segmentation, U-Net stands out as a commonly employed technique. Its unique U-shaped architecture incorporates skip connections, allowing the decoder to merge high-level semantic feature maps with low-level detailed feature maps from the encoder.

However, there is a common misconception that the success of U-Net is solely tied to its U-shaped structure, leading to the emergence of several U-Net-based models. The term "U" encompasses two distinct architectural paths: the encoder (contracting layer) on the left and the decoder (expanding layer) on the right. The encoder performs downsampling to reduce the input matrix's size while increasing the number of feature maps. At the same time, the decoder path works in reverse to restore the matrix to its original size by decreasing the number of feature maps. As a result, a pixel-wise comparison of segmentation results against the ground truth is feasible. U-Net facilitates the flow of feature maps from each level of the contracting path to the corresponding level in the expanding path, enabling the classifier to analyze characteristics of varying sizes and complexities. Furthermore, UNet architecture is complex to train and requires much time for training execution [16][17].

This study proposes a teledentistry system, as shown in Figure 1, which utilizes the pre-trained segmentation model. The input image was captured by an intraoral camera and transformed into input tensors. The Half U-Net Model Controller will generate the ground truth tensors based on the input images. The web server will transmit the generated ground truth, which will be stored in teledentistry system databases. Therefore, this research proposed a simplified dental caries segmentation for the teledentistry system.

METHOD

Material

The U-Net modification architectures were implemented since the original model was trained on a machine equipped with an Intel (R) Core i5-6300HQ CPU, 16GB RAM, 512GB SSD, and an NVidia GeForce GTX 960M with 4GB VRAM. Recognizing the need for scalability and enhanced performance, several improvements were made to adapt the model to more powerful hardware configurations.

The model was built with PyTorch in the Jupyter Notebook environment. This framework and platform combination enabled a versatile and efficient development environment. Furthermore, GPU acceleration was used to improve the computational speed and efficiency of the research, allowing for quicker execution of the calculation processes involved in the model's activities.

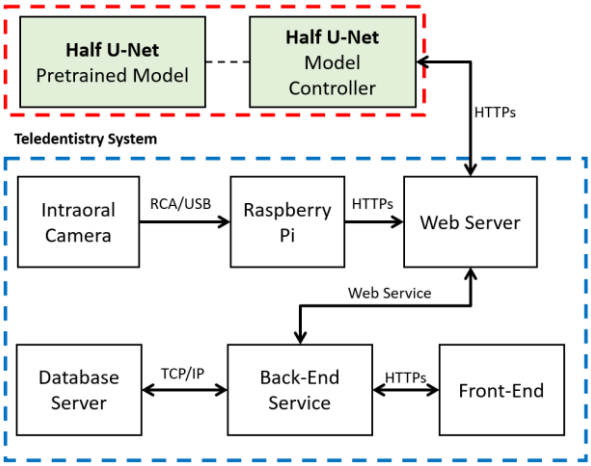

Figure 1. Teledentistry System on Clinic using Half U-Net Model

Methods

This study gives the dataset distribution 67% as the training set, 23% as the validation set, and 10% as the evaluation set in order to deliver stable model performance that avoids overfitting or underfitting the UNet model. The dataset contains 200 dental care records compiled using an annotation tool. Figure 2 depicts the research approaches utilized with the dental caries dataset and underlying Ground Truth.

The augmentation approach depicted in Figure 2 includes scaling the input picture from its original resolution to 128x128 pixels. Then, we utilize 'tf.reduce_mean', a function that computes the mean of tensor elements along given axes.

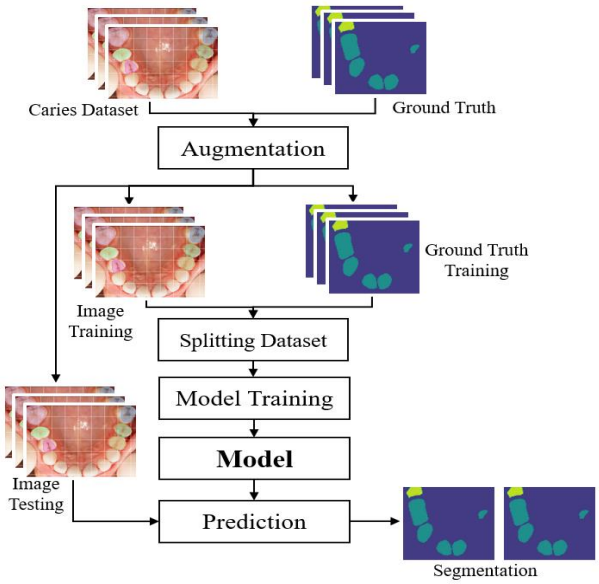

Figure 2. Research Method

It is a basic operation that is used in many neural network activities, including loss computation and performance evaluation. The model training process is divided into three stages: training, validation, and evaluation. Each stage serves a distinct purpose and contributes to ensuring that the trained model can generalize effectively to unseen data and perform optimum for the task. Training Stage: Using labeled data, adjust model parameters to reduce the discrepancy between predictions and ground truth. Validation Stage: evaluating the model's performance on a distinct dataset to track progress and avoid overfitting. Evaluation Stage: evaluate the model's real-world capabilities using an unknown test dataset to get impartial performance metrics. The augmentation approach depicted in Figure 2 includes scaling the input picture from its original resolution to 128x128 pixels.

Then, we utilize 'tf.reduce_mean', a function that computes the mean of tensor elements along given axes. It is a basic operation that is used in many neural network activities, including loss computation and performance evaluation. The model training process is divided into three stages: training, validation, and evaluation. Each stage serves a distinct purpose and contributes to ensuring that the trained model can generalize effectively to unseen data and perform optimum for the task. Training Stage: Using labeled data, adjust model parameters to reduce the discrepancy between predictions and ground truth. Validation Stage: evaluating the model's performance on a distinct dataset to track progress and avoid overfitting. Evaluation Stage: evaluate the model's real-world capabilities using an unknown test dataset to get impartial performance metrics.

As a converter, full-scale skip connections transform the interconnection between the encoder and decoder (including its sub-network). The primary distinction between the U-Net and the Half-UNet is the number of decoder blocks employed. We deleted certain decoder blocks from the Half-UNet to minimize the model complexity and parameters, making it a smaller version of the UNet design. As the number of decoder blocks is reduced, the number of convolutional layers and parameters in the Half-UNet model is reduced as compared to the original U-Net. Figure 3 represents the distinction between the U-Net and the Half-UNet. Figure 3 illustrates the feature map construction of UNet encoder and decoder. Each denotes as X_{En}^{i} and X_{De}^{i}, let i as an index in the down-sampling layer along the encoder, X_{De}^{i} can be computed as:

$$X_{De}^{i} = \begin{cases} X_{En}^{i}, i=N \\ H([C(D(X_{En}^{k}))_{k=1}^{i-1}, C(X_{En}^{i}), C(U(X_{De}^{k}))_{k=i+1}^{N}]), i=i,\ldots N-1 \end{cases} \quad (1)$$

where $H(.)$ is the feature aggregation mechanism, which consists of a batch normalization and the activation function. The function $C(.)$ denotes feature map operation containing up-sampling $U(.)$ and down-sampling $D(.)$ operations.

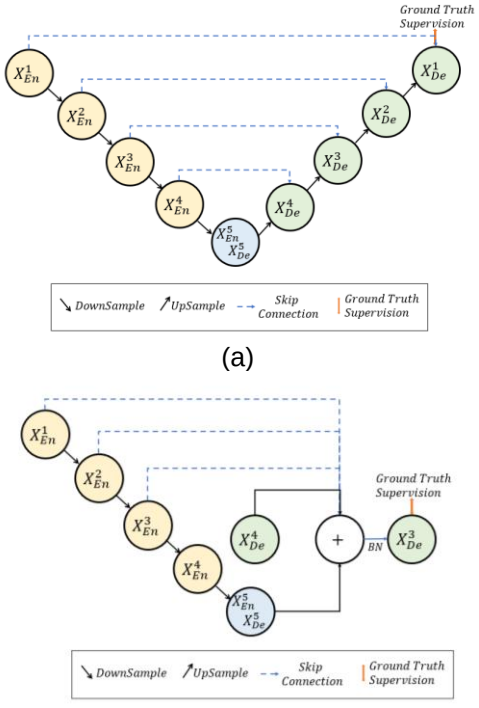

Figure 3. Architecture of (a) UNet [18][19] and (b) Half-UNet

A set of inter-encode-decode skip connections transmits the low-level tensor from X_{En}^{i} mini-encoder into X_{En}^{i+1}, where a non-overlapping max pooling operation is executed. In UNet, the decoder skip connection uses bilinear interpolation to transport high-level tensors from decoder X_{De}^{i} to decoder X_{De}^{i+1}. The UNet decoder has a more detailed feature map operation than the Half-UNet decoder, which displays a symmetric decoder. Therefore, the number of UNet parameter in i^{th} decoder stage can be formulated as:

$$P_{U-De}^{i} = D_f \times D_f [d(X_{De}^{i+1}) \times d(X_{De}^{i}) + d(X_{De}^{i})^2] + d(X_{En}^{i} + X_{De}^{i}) \times d(X_{De}^{i})] \quad (2)$$

where D_f is the kernel size of the convolution, $d(.)$ is the node depth.

The Dice coefficient can be employed to evaluate the segmentation performance, measuring the degree of overlap between the model's prediction and the ground truth areas. It is computed by dividing the intersection area of the two regions by the sum of their areas. A higher Dice coefficient indicates that the model's predictions closely align with the ground truth, resulting in improved picture segmentation outcomes. The Dice coefficient is calculated using the following formula when the model's prediction result area is denoted as P and the ground truth of breast lumps is denoted as [19]–[22]:

$$Dice = \frac{2|P \cap M|}{|P| + |M|} \quad (3)$$

RESULTS AND DISCUSSION

In this paper, we propose the same encoder blocks for whole models. We simplify the Half-UNet model with decoder X_{De}^{4} containing two and three blocks. FLOPs is an abbreviation for "Floating-Point Operations per Second." It is a unit of measurement used to characterize a computer system's performance, notably in terms of the number of floating-point arithmetic operations it can do in one second. Floating-point operations are mathematical computations that use fractional parts of numbers (decimal numbers) and floating-point representation, which allows the position of the decimal point to fluctuate (float) as needed. Typical floating-point operations include addition, subtraction, multiplication, division, and other sophisticated mathematical operations using real numbers.

Table 1. Model Architectures

Model	X^{i}_{En} (blocks)	X^{i}_{De} (blocks)	FLOPs
UNet	5	5	5×
Half-UNet (X^{3}_{De})	5	3	1.7×
Half-UNet (X^{4}_{De})	5	2	1×

Table 1 shows the comparison of the model architectures that measure using FLOPs.

In this paper, we evaluate the proposed approach to the prior state-of-the-art model. The U-Net architecture is created using numerous scenarios in order to produce multiple alternative models, which are then evaluated for loss amongst one another and with the proposed model. These U-Net modification architectures are carried out since the original U-Net model has been trained using Processor Intel (R) Core i5-6300HQ, 16GB RAM, 512GB SSD, and NVidia GeForce GTX 960M with 4GB VRAM. Table 2 shows the performance comparison between UNet, Half-UNet (X^{4}_{De}), and Half-UNet (X^{3}_{De}).

Based on Table 2, the UNet and Half-UNet were successfully trained using the Dental Caries dataset. The dice coefficient measures network segmentation performance. The UNet Model's simplification can preserve the model's performance in segmenting the actual images and ground truth against predicted ground truth. However, based on the results of the UNet Model simplification experiment, it has not been able to improve the model's performance significantly. Although the reduction of the decoder layer on UNet to the level of blocks 3 (X^{3}_{De}) and blocks 4 (X^{4}_{De}) can be performed for image segmentation of Dental Caries. After down sampling, the method of doubling the number of channels improves the channel counts for high-level semantic features. Figure 4 represents the segmentation result generated by the proposed model.

Table 2. Performance Comparison

Model	Train Loss (%)	Val Loss (%)	Dice	Time Exec. (hours)
UNet	1.12	0.88	0.81	6.76
Half-UNet (X^{4}_{De})	0.78	0.64	0.83	2.97
Half-UNet (X^{3}_{De})	0.94	0.64	0.82	3.13

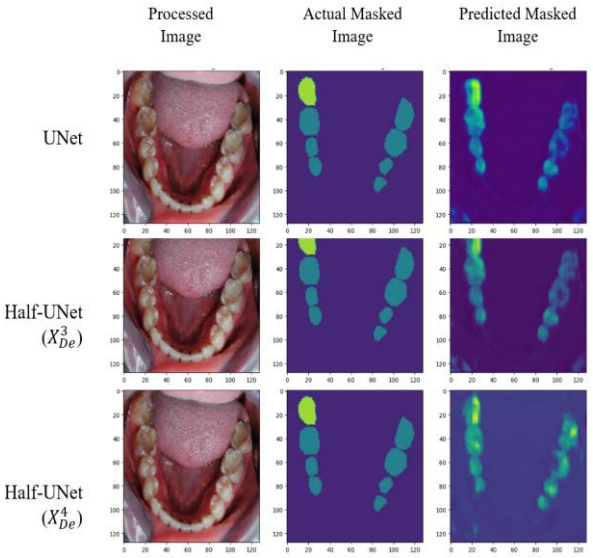

Figure 4. Model Test

The Half-UNet structural model outperforms the U-shaped structural model in terms of efficiency and segmentation ability. Because bilinear upsampling and addition are linear processes, no parameters or computations are created on the left side of the Half-UNet sub-network. We also use batch normalization to avoid model from internal covariate shifts. Without installing a dropout layer, it can also operate as a regularize to decrease generalization error and avoid overfitting. Batch Normalization is performed immediately after convolution and before ReLU to decrease computation [23, 24, 25, 26, 27]. In the Half-UNet concatenate the feature maps at the lowest possible cost. In Figure 5, we implement the Half-UNet (X^{4}_{De}) in Teledentistry System.

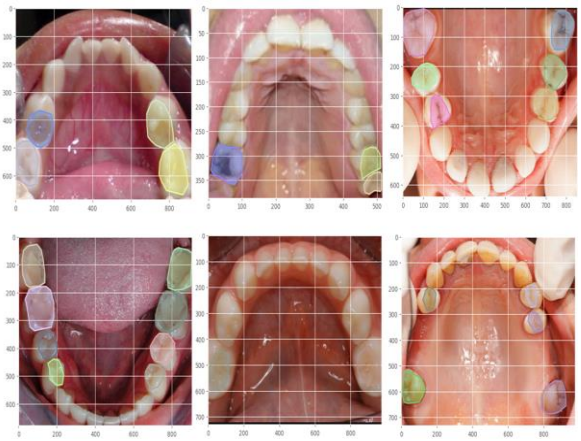

Figure 5. Half-UNet (X^{4}_{De}) in Teledentistry System

CONCLUSION

In this study, the simplification of U-Net architectures is carried out since the original U-Net model has been trained using Processor Intel (R) Core i5-6300HQ, 16GB RAM, 512GB SSD, and NVidia GeForce GTX 960M with 4GB VRAM. The simplification proved that the feature reduction of the decoder layers. We simplified the original UNet decoder layers into the level of blocks 3 (X_{De}^{3}) and blocks 4 (X_{De}^{4}). It can be performed for image segmentation of Dental Caries. In terms of efficiency and segmentation capabilities, the Half-UNet structural model surpasses the U-shaped structural model. In this study, batch Normalization is applied immediately after convolution and before ReLU to reduce computation, generalization error, and an overfitting model. Based on the experiment, the simplification of the UNet architecture outperformed using Half-UNet X_{De}^{4} 0.83% of the dice coefficient. Therefore, the Half-UNet (X_{De}^{4}) has been implement in Teledentistry System.

ACKNOWLEDGMENT

The successful completion of this research would not have been possible without the generous support and cooperation of the Department of Electrical Engineering and the Research Center of Universitas Mercu Buana, along with the Department of Electrical Engineering at Politeknik Negeri Jakarta. The Authors thank these esteemed institutions for providing valuable resources, guidance, and encouragement throughout the research journey. Their unwavering commitment has been pivotal in the realization of this project's objectives.

REFERENCES

[1] M. Sahu and R. Dash, "A Mask-based Cavity Detection Model for Dental X-ray Image," *2020 International Conference on Computer Science, Engineering and Applications (ICCSEA)*, Gunupur, India, 2020, pp. 1-4, doi: 10.1109/ICCSEA49143.2020.9132908.

[2] T. M. Kadarina, Z. Iklima, R. Priambodo, Riandini, and R. N. Wardhani, “Dental caries classification using depthwise separable convolutional neural network for teledentistry system,” *Bulletin of Electrical Engineering and Informatics*, vol. 12, no. 2, pp. 940–949, 2023, doi: 10.11591/eei.v12i2.4428.

[3] V. Majanga and S. Viriri, “A Survey of Dental Caries Segmentation and Detection Techniques,” *The Scientific World Journal*, vol. 2022, 2022, doi: 10.1155/2022/8415705.

[4] M. Irving, R. Stewart, H. Spallek, and A. Blinkhorn, “Using teledentistry in clinical practice as an enabler to improve access to clinical care: A qualitative systematic review,” *Journal of Telemedicine and Telecare*, vol. 24, no. 3, pp. 129–146, 2018, doi: 10.1177/1357633X16686776.

[5] H. Zhu, Z. Cao, L. Lian, G. Ye, H. Gao, and J. Wu, “CariesNet: a deep learning approach for segmentation of multi-stage caries lesion from oral panoramic X-ray image,” *Neural Computing and Applications*, vol. 2, 2022, doi: 10.1007/s00521-021-06684-2.

[6] J. H. Lee, D. H. Kim, S. N. Jeong, and S. H. Choi, “Detection and diagnosis of dental caries using a deep learning-based convolutional neural network algorithm,” *Journal of Dentistry*, vol. 77, pp. 106–111, Oct. 2018, doi: 10.1016/j.jdent.2018.07.015.

[7] A. Sonavane, R. Yadav, and A. Khamparia, “Dental cavity classification of using convolutional neural network,” *IOP Conf. Ser. Mater. Sci. Eng.*, vol. 1022, no. 1, 2021, doi: 10.1088/1757-899X/1022/1/012116.

[8] D. Saini, R. Jain and A. Thakur, "Dental Caries early detection using Convolutional Neural Network for Tele dentistry," *2021 7th International Conference on Advanced Computing and Communication Systems (ICACCS)*, Coimbatore, India, 2021, pp. 958-963, doi: 10.1109/ICACCS51430.2021.9442001.

[9] A. Laishram and K. Thongam, "Detection and Classification of Dental Pathologies using Faster-RCNN in Orthopantomogram Radiography Image," *2020 7th International Conference on Signal Processing and Integrated Networks (SPIN)*, Noida, India, 2020, pp. 423-428, doi: 10.1109/SPIN48934.2020.9071242.

[10] F. Oztekin *et al.*, “An Explainable Deep Learning Model to Prediction Dental Caries Using Panoramic Radiograph Images,” *Diagnostics*, vol. 13, no. 2, 2023, doi: 10.3390/diagnostics13020226.

[11] B. Duman, “A Novel Deep Learning-Based Approach for Segmentation of Different Type Caries Lesions on Panoramic Radiographs,” *Diagnostics*, vol. 13, no. 2, pp. 202, 2023, doi: 10.3390/diagnostics13020202.

[12] M. P. Muresan, A. R. Barbura, and S. Nedevschi, “Teeth Detection and Dental Problem Classification in Panoramic X-Ray Images using Deep Learning and Image Processing Techniques,” *Proc. - 2020 IEEE 16th Int. Conf. Intell. Comput. Commun.*

Process. ICCP 2020, pp. 457–463, 2020, doi: 10.1109/ICCP51029.2020.9266244.
[13] O. Baydar, I. Różyło-Kalinowska, K. Futyma-Gąbka, and H. Sağlam, "The U-Net Approaches to Evaluation of Dental Bite-Wing Radiographs: An Artificial Intelligence Study," *Diagnostics*, vol. 13, no. 3, 2023, doi: 10.3390/diagnostics13030453.
[14] S. Lin, X. Hao, Y. Liu, D. Yan, J. Liu, and M. Zhong, "Lightweight deep learning methods for panoramic dental X-ray image segmentation," *Neural Computing and Applications*, Apr. 2022, doi: 10.1007/S00521-022-08102-7.
[15] A. Fariza, A. Z. Arifin, and E. R. Astuti, "Automatic Tooth and Background Segmentation in Dental X-ray Using U-Net Convolution Network," *2020 6th Int. Conf. Sci. Inf. Technol. Embrac. Ind. 4.0 Towar. Innov. Disaster Manag. ICSITech 2020*, no. September 2021, pp. 144–149, 2020, doi: 10.1109/ICSITech49800.2020.9392039.
[16] A. A. Pravitasari *et al.*, "UNet-VGG16 with transfer learning for MRI-based brain tumor segmentation," *Telkomnika (Telecommunication Comput. Electron. Control.*, vol. 18, no. 3, pp. 1310–1318, 2020, doi: 10.12928/telkomnika.v18i3.14753.
[17] S. Sukegawa *et al.*, "Deep Neural Networks for Dental Implant System Classification," *Biomolecules,* vol. 10, no. 7, pp. 984, Jul. 2020, doi: 10.3390/BIOM10070984.
[18] H. Huang *et al.*, "UNet 3+: A Full-Scale Connected UNet for Medical Image Segmentation," *ICASSP, IEEE Int. Conf. Acoust. Speech Signal Process. - Proc.*, vol. 2020-May, no. iii, pp. 1055–1059, 2020, doi: 10.1109/ICASSP40776.2020.9053405.
[19] H. Lu, Y. She, J. Tie, and S. Xu, "Half-UNet: A Simplified U-Net Architecture for Medical Image Segmentation," *Frontiers in Neuroinformatics*, vol. 16, no. June, pp. 1–10, 2022, doi: 10.3389/fninf.2022.911679.
[20] S. Sukegawa *et al.*, "Deep neural networks for dental implant system classification," *Biomolecules*, vol. 10, no. 7, pp. 1–13, 2020, doi: 10.3390/biom10070984.
[21] F. Oztekin *et al.*, "An Explainable Deep Learning Model to Prediction Dental Caries Using Panoramic Radiograph Images," *Diagnostics*, vol. 13, no. 2, Jan. 2023, doi: 10.3390/DIAGNOSTICS13020226.
[22] F. Li, X. Liu, Y. Yin, and Z. Li, "DDR-Unet: A High-Accuracy and Efficient Ore Image Segmentation Method," *IEEE Transactions on Instrumentation and Measurement*, vol. 72, 2023, doi: 10.1109/TIM.2023.3317480.
[23] E. Ihsanto, K. Ramli, D. Sudiana, and T. S. Gunawan, "An efficient algorithm for cardiac arrhythmia classification using ensemble of depthwise separable convolutional neural networks," *Applied Sciences*, vol. 10, no. 2, 2020, doi: 10.3390/app10020483.
[24] Z. Iklima, T. M. Kadarina, and R. Priambodo, "Reduction of Feature Extraction for COVID-19 CXR using Depthwise Separable Convolution Network," *Journal of Electronics, Electromedical Engineering, and Medical Informatic*, vol. 4, no. 4, pp. 204–209, 2022, doi: 10.35882/jeeemi.v4i4.255.
[25] Z. Iklima, T. M. Kadarina, and E. Ihsanto, "Realistic image synthesis of COVID-19 chest X-rays using depthwise boundary equilibrium generative adversarial networks," *International Journal of Electrical and Computer Engineering (IJECE)*, vol. 12, no. 5, pp. 5444–5454, 2022, doi: 10.11591/ijece.v12i5.pp5444-5454.
[26] K. Aziz, I. K. Trisiawan, K. D. Suyasmini, Z. Iklima, M. Yunita, "Multilabel image analysis on Polyethylene Terephthalate bottle images using PETNet Convolution Architecture," *SINERGI*, vol. 27, no. 2. pp. 163-170, 2023, doi: 10.22441/sinergi.2023.2.003
[27] A. Ashraf, A. Sophian, A. A. Shafie, T. S. Gunawan, N. N. Ismail, A. A. Bawono, "Detection of road cracks using Convolutional Neural Networks and Threshold Segmentation," *Journal of Integrated and Advanced Engineering (JIAE)*, vol. 2, no. 2, pp. 123-134, 2022, doi: 10.51662/jiae.v2i2.82